Positron emission tomography reporter gene strategy for use in the central nervous system

Tom Haywood[a], Corinne Beinat[a], Gayatri Gowrishankar[a], Chirag B. Patel[a,b], Israt S. Alam[a], Surya Murty[a], and Sanjiv Sam Gambhir[a,1]

[a]Department of Radiology, Molecular Imaging Program, Stanford University, Stanford, CA 94305; and [b]Department of Neurology and Neurological Sciences, Stanford University, Stanford, CA 94305

Edited by Michael E. Phelps, University of California, Los Angeles, CA, and approved April 29, 2019 (received for review February 6, 2019)

There is a growing need for monitoring or imaging gene therapy in the central nervous system (CNS). This can be achieved with a positron emission tomography (PET) reporter gene strategy. Here we report the development of a PET reporter gene system using the PKM2 gene with its associated radiotracer [^{18}F]DASA-23. The PKM2 reporter gene was delivered to the brains of mice by adeno-associated virus (AAV9) via stereotactic injection. Serial PET imaging was carried out over 8 wk to assess PKM2 expression. After 8 wk, the brains were excised for further mRNA and protein analysis. PET imaging at 8 wk post-AAV delivery showed an increase in [^{18}F]DASA-23 brain uptake in the transduced site of mice injected with the AAV mice over all controls. We believe PKM2 shows great promise as a PET reporter gene and to date is the only example that can be used in all areas of the CNS without breaking the blood–brain barrier, to monitor gene and cell therapy.

reporter gene | positron emission tomography (PET) | PKM2 | [18F]DASA-23 | adeno-associated virus

The accurate monitoring of gene therapies for diseases of the central nervous system (CNS) is currently a challenging task, due to a lack of noninvasive methods (1). As gene/cell therapy approaches continue to grow in use and popularity, with the first in vivo human genome editing trial recently taking place (2), a robust method for monitoring their delivery, efficacy, and localization is vital (3). One such method ideally suited to monitor gene therapies and their expression is positron emission tomography (PET) reporter gene systems (4, 5). PET is a noninvasive molecular imaging technique that is used to study and visualize human physiology by detection of positron-emitting radiopharmaceuticals. An important advantage of PET as an imaging technique is that it provides cellular and functional information that cannot be detected with structural imaging modalities such as magnetic resonance imaging (MRI) or computed tomography (CT) (6). A gene therapy, which can be monitored noninvasively with PET, would require the incorporation of an additional reporter gene into the vector containing the therapeutic gene of interest. Transcription of this reporter gene followed by translation of the mRNA provides the reporter protein, which can be detected by a corresponding high-affinity PET radiotracer. Thus, the level of measured radioactivity is a direct reflection of the reporter gene and therefore an indirect but proportional measure of therapeutic gene expression at a particular site (7).

When developing a new PET reporter gene system, a number of considerations must be taken into account: (*i*) the gene should already be present in mammalian cells to prevent an immune response, but not expressed in the region(s) of interest; (*ii*) the gene and promoter should be small enough to fit into a delivery vector; (*iii*) the image signals should correlate with levels of reporter gene mRNA and protein; (*iv*) the protein product should not cause an immune response or downstream biological response; (*v*) the signal should only be detected in regions where the reporter gene is expressed; (*vi*) expression of the reporter gene should not significantly perturb underlying cell biology (8). Regarding a CNS PET reporter gene system, the radiotracer must also be able to cross the intact blood–brain barrier (BBB) freely while at low concentration, to reach the sites of the gene expression.

With these considerations in mind, a new PET reporter gene system that could be used to monitor gene therapy (and cell therapies) of CNS diseases was sought. The PKM2 protein is an isoform of pyruvate kinase (PK) involved in the final rate-limiting step of glycolysis (9). PKM2 protein is found in the majority of human cells with the exception of muscle, liver, and most importantly, with no expression in the healthy brain (10). In recent years, PKM2 protein has been explored as a potential target for cancer imaging as it is up-regulated in a wide range of human cancers, largely due to its role in metabolism and the Warburg effect (11). To date, radiolabeled DASA-23 is the only radiotracer for the PKM2 protein. It has shown great potential as an effective imaging agent in preclinical studies since it is able to cross the BBB freely and image tumors in the CNS, while having very low uptake in the brain of healthy mice as shown in biodistribution studies (12–14). [^{18}F]DASA-23 is currently undergoing a phase 1 clinical trial at Stanford University (NCT03539731), evaluating PKM2 expression in patients with intracranial tumors or recurrent glioblastoma (15). The DASA-23 and other DASA analogs have been shown to bind to a pocket at the interface of the PKM2 subunit interaction; this interaction stabilizes a tetrameric conformation state (16). This stabilization of the tetrameric state shifts the equilibrium; however, the binding is reversible rather than irreversible.

Materials and Methods

Cell Lines, Culture Conditions, and Transfection Procedures. HeLa cell lines (ATCC) were used for all in vitro studies. Cells (4×10^5) were plated in six-well plates containing DMEM supplemented with 10% FBS and 1% Gibco

Significance

With any new treatment it is imperative the medical community has a way to monitor its effectiveness, tracking its location, monitoring its expression, and observing off-target effects. Gene/cell therapy is no exception. The growing number of studies creates a need to monitor them more accurately. A number of PET reporter gene systems have been reported; however, they have limitations, including regions of high endogenous gene expression in the central nervous system (CNS), low specificity, or endogenous expression of the reporter gene in microglia. One of these systems has been used in the clinical setting; however, its associated imaging agent lacks blood–brain barrier penetration. Our approach aims to overcome these limitations and facilitate monitoring of gene/cell therapy in the CNS.

Author contributions: S.S.G. conceived the idea for the study; T.H., G.G., and S.S.G. designed research; T.H., C.B., G.G., C.B.P., I.S.A., and S.M. performed research; C.B. contributed new reagents/analytic tools; T.H. and S.S.G. analyzed data; and T.H. and S.S.G. wrote the paper.

The authors declare no conflict of interest.

This article is a PNAS Direct Submission.

[1]To whom correspondence may be addressed. Email: sgambhir@stanford.edu.

This article contains supporting information online at www.pnas.org/lookup/suppl/doi:10.1073/pnas.1901645116/-/DCSupplemental.

Published online May 23, 2019.

antibiotic-antimycotic consisting of 10,000 units/mL of penicillin, 10,000 μg/mL of streptomycin, and 25 μg/mL of Gibco amphotericin B (Thermo Fisher Scientific). The cells were plated 1 d before transfection. Transfections were performed using Lipofectamine 3000 reagent (Thermo Fisher Scientific) at a concentration of 7.5 μL per well with 2.5 μg/mL of plasmid. For transfections where the PKM2 plasmid concentration was <2.5 μg/mL, the control GFP plasmid (Vector Builder) was used to maintain a constant total plasmid concentration. Cells were incubated for 48 h posttransfection before further studies.

Radiolabeling. Synthesis of [^{18}F]DASA-23 was performed on a GE TRACERLab FXFN module, using [^{18}F]fluoride in [^{18}O]H_2O as the radiolabeling reagent as previously reported by our laboratory (13).

Cell Uptake Studies. Forty-eight hours after transfection, fresh, prewarmed growth media containing 0.185 MBq of [^{18}F]DASA-23 was added to individual wells (1 mL per well, six-well plates). Cells were incubated with [^{18}F]DASA-23 at 37 °C and 5% CO_2 for 30 and 60 min. At the indicated time points, plates were placed on ice, washed twice with ice-cold PBS (2 mL per well), and lysed with radioimmunoprecipitation assay (RIPA) buffer (Thermo Fisher Scientific; 500 μL). Cell lysates (300 μL) were transferred to gamma counting tubes, and decay-corrected radioactivity was determined on a gamma counter (Cobra II Auto-Gamma Counter; Packard Biosciences). For efflux studies, cells were incubated with radiotracer for 60 min and washed twice with ice-cold PBS before subsequent incubation at 37 °C in fresh, radiotracer-free growth media for a further 30 min. Plates were placed on ice, washed twice with ice-cold PBS, lysed with RIPA buffer (500 μL), transferred (300 μL) to gamma counting tubes, and counted. The lysates were subsequently used after radioactive decay for protein quantitation with a bicinchoninic acid (BCA) 96-well plate assay (Thermo Fisher Scientific). In addition, standards from the [^{18}F]DASA-23 solution (100 μL, 0.185 MBq/mL) added to cells were counted to quantitate percentage radiotracer uptake. In vitro quantitative PCR (qPCR) analysis is described in *SI Appendix*.

Stereotactic Injection of AAV. Six- to eight-wk old female BALB/c mice (Charles River, $n = 15$) were anesthetized (2% isoflurane in oxygen), administered eye ointment (LubriFresh P.M., Major Pharmaceuticals), analgesia buprenorphine [0.1 mg/kg, s.c. (SQ)], and also saline 0.5 mL SQ. The mice were then placed in a stereotactic frame (KOPF, 900LS) and injected unilaterally with 3 μL AAV9-EF1A-PKM2 (VectorBuilder) (*SI Appendix*, Fig. S2), concentrated by the Stanford in-house core, 1.18×10^{13} vg/mL (viral genome/milliliter), ($n = 7$), or 2 μL AAV9-EF1A-LUC2 (VectorBuilder, packaged by the Stanford in-house core, 4.25×10^{13} vg/mL, $n = 4$), or 2.5 μL saline ($n = 4$), into the ventral tegmental area through a burr hole in the skull (3.3 mm posterior to bregma, 0.3 mm to the right of midline, and 4.1 mm deep from the top of the skull). Healthy control mice were left noninjected ($n = 4$). All experimental procedures involving animals were approved by the Stanford University Institutional Animal Care and Use Committee, protocol no. 32748

Animal Imaging. Small animal PET/CT imaging was repeated periodically over 8 wk. Dynamic scans were acquired after a bolus i.v. injection of 7.4–11.1 MBq of [^{18}F]DASA-23 into mice. T2-weighted MR images were acquired 30 d postinjection in the coronal planes through the region of transduction. The expression of Firefly luciferase in mice transfected with AAV-Luc 2 was imaged using bioluminescent imaging (BLI) 14, 33, and 56 d post-AAV injection. Full details of animal imaging procedures, ex vivo autoradiography, and histopathology are reported in *SI Appendix*. Data from all imaged mice have been reported unless otherwise stated.

Statistical Analyses. Data were expressed as means ± SD. For the analysis of [^{18}F]DASA-23 uptake in brain regions (see Fig. 3C), statistical significance between different groups was determined by analysis of variance (ANOVA), followed by Tukey's multiple comparison test. Correlation analysis using Spearman's rank correlation, linear regression, statistical significance, and 95% confidence levels was determined using Prism software for Windows (v.7.03; GraphPad Software). Differences between groups were considered significant if $P \leq 0.05$, ns $P > 0.05$, *$P \leq 0.05$, **$P \leq 0.01$, ***$P \leq 0.001$, ****$P \leq 0.0001$.

Results

Cell Culture Studies. After a 30-min incubation, [^{18}F]DASA-23 showed sixfold higher accumulation in cells transfected with PKM2 plasmids, compared with nontransfected HeLa cells and those transfected with a control plasmid, 133.7 ± 13.0% vs. 21.5 ± 14.2% and 23.6 ± 5.8% of tracer uptake per milligram of protein respectively ($P < 0.001$ and $P \leq 0.0001$). There was no statistical significance between the two control samples ($P = 0.9938$). Efflux studies carried out at 30 min showed a 43% decrease in the tracer uptake compared with the 60-min incubation wells (Fig. 1).

In PKM2-transfected HeLa cells, a strong positive linear correlation between accumulation of [^{18}F]DASA-23 and concentration of plasmid used for transfection of the PKM2 gene was observed ($R^2 = 0.92$, $P < 0.01$; Fig. 2*A*). HeLa cells expressed increasing levels of PKM2 mRNA normalized to β-actin, when transfected with higher levels of plasmid containing the PKM2 gene ($R^2 = 0.95$, $P < 0.01$; Fig. 2*B*). There was also a good correlation between levels of [^{18}F]DASA-23 tracer accumulation as a function of PKM2 mRNA levels ($R^2 = 0.91$, $P < 0.05$; Fig. 2*C*).

Small Animal Studies. Two days before injection of the AAV carrying PKM2 or Luc2, a [^{18}F]DASA-23 PET was carried out to determine the baseline image. ROIs of approximate equal size were drawn in the region of the injection site and a corresponding ROI on the contralateral side. Statistically there was no difference in [^{18}F]DASA-23 accumulation between either side of the brain (1.03 ± 0.10, $n = 4$). Two days poststereotactic injection of the AAV-EF1A-PKM2 into the brain, the expression of PKM2 in mice was imaged using PET. These initial images showed no sign of increased uptake of [^{18}F]DASA-23 with a transduced site to control ratio (1.04 ± 0.12, $n = 3$) (Fig. 3*A*). Two weeks after viral delivery, a third PET imaging study was carried out. No statistical increase in uptake was present although a small increase in signal was visible in some of the transduced mice over the contralateral side, with the viral delivery site ROI compared with contralateral ROI ratio (1.07 ± 0.12, $n = 3$). Scans carried out at 35 d postviral injection showed a clear increase in [^{18}F]DASA-23 signal in most of the transduced mice (five out of seven mice scanned), with a transduced site ROI to contralateral ROI ratio of 1.59 ± 0.45 ($n = 3$), although this was not statistically significant from the previral delivery scan ($P = 0.195$). One of the imaged mice injected with AAV-PKM2 showed no discernible signal even after 35 d. Further PET imaging at 57 d showed further

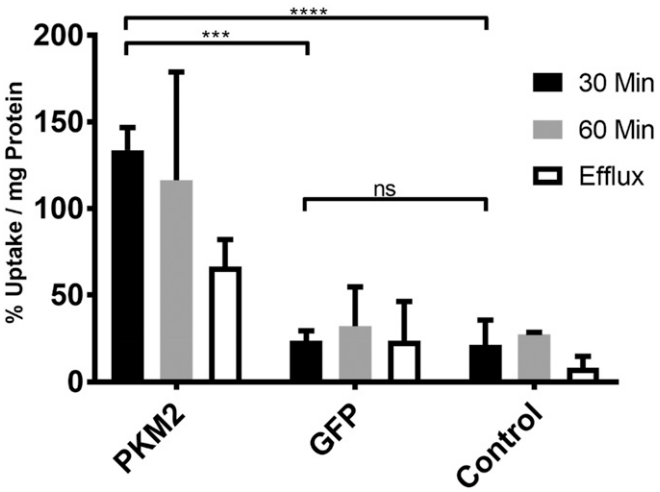

Fig. 1. [^{18}F]DASA-23 accumulation in HeLa cells transfected with a plasmid containing the PKM2 gene, GFP gene, and nontransfected control cells. Radiotracer accumulation was measured after 30 and 60 min of tracer incubation, as well as 60 min incubation followed by 30 min efflux ($n = 3$, error bars represent SD); 30 min PKM2 vs. GFP ($P < 0.001$, ***), PKM2 vs. control ($P < 0.0001$, ****), GFP vs. control ($P > 0.05$, ns). 60 min PKM2 vs. GFP ($P < 0.01$, **), PKM2 vs. control ($P < 0.01$, **), GFP vs. control ($P > 0.05$, ns). Efflux PKM2 vs. GFP ($P > 0.05$, ns), PKM2 vs. control ($P < 0.05$, *), GFP vs. control ($P > 0.05$, ns).

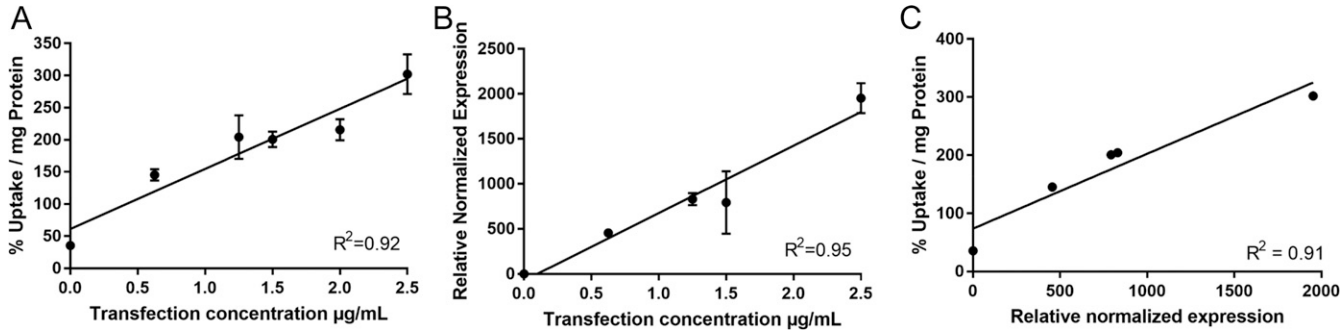

Fig. 2. Correlation between [^{18}F]DASA-23 accumulation in cells and PKM2 mRNA levels. HeLa cells were transfected with six different plasmid titers. Cells were subsequently incubated with [^{18}F]DASA-23 for 60 min and assayed for [^{18}F]DASA-23 accumulation, PKM2 mRNA and β-actin mRNA levels. (*A*) [^{18}F]DASA-23 normalized accumulation as a function of plasmid titer. (*B*) PKM2 mRNA levels (normalized to β-actin levels) in transfected HeLa cells as a function of plasmid titer. (*C*) [^{18}F]DASA-23 normalized accumulation as a function of PKM2 mRNA levels (normalized to β-actin levels). R^2 values shown in the graphs were determined by linear regression calculations performed in GraphPad.

increases from 35 d, with the increase in PET signal much more visually apparent (Fig. 3A) in those that showed a signal, with a viral injected site to control ROI ratio (2.24 ± 0.52, $n = 3$). This was statistically significant from the previral delivery scan ($P = 0.0025$). In those mice that did not show signal at 35 d, still no appreciable signal was seen at 57 d. These four imaging time points showed a steady increase in [^{18}F]DASA-23 uptake over time, indicating an increased expression of PKM2 delivered via the AAV (Fig. 3*A*). Time activity curves (TACs) at 30 min after [^{18}F]DASA-23 tracer injection show an increase in uptake in areas of the brain (Fig. 3*B*). An increase (79.8–147%) in [^{18}F]DASA-23 accumulation was seen in mice transduced ($n = 4$) with AAV compared with all control groups; no injection (79.8%, $P = 0.0007$, $n = 4$), contralateral (89.4%, $P = 0.0004$, $n = 4$), Luc2 (146.0%, $P < 0.0001$, $n = 4$), sham (147.0%, $P = 0.0003$, $n = 2$) (Fig. 3*C*). None of the control groups (Luc2 AAV, sham saline injection, no injection) showed any measurable increase in [^{18}F]DASA-23 uptake in the brain during PET imaging studies. Dynamic images of AAV-PKM2 transduced mice show accumulation of [^{18}F]DASA-23 in the brain over the imaging time course (*SI Appendix*, Movies S1 and S2).

Mice transfected with AAV-Luc2 (mice 1–3, 5) and imaged using BLI all showed a bioluminescent signal from 33 d onwards (*SI Appendix*, Fig. S1). One mouse transduced with AAV-PKM2 (mouse 4) showed no bioluminescent signal at any imaging time point as expected.

PKM2 Expression Validation. Immediately after the 57 d PET scan, all mice were perfused, killed, and their brains excised. Brains were randomly divided and used for ex vivo autoradiography and immunofluorescence ($n = 2$ with AAV, $n = 4$ no injection, $n = 2$ Luc2, $n = 1$ sham saline injection). Autoradiography of excised brains transduced with PKM2 revealed distinct regions of localized radioactivity (Fig. 4*C*), consistent with areas of increased signal seen during PET imaging. Control sections showed no distinguishable areas of increased radioactivity in the brain, and a similar level of radioactivity to nontransduced areas of the transduced mice. Analysis of the autoradiogram using ImageJ (version 1.51j8) (Fig. 4*C*) showed a statistically significant ($P < 0.0001$) difference between the mean pixel gray value for a transduced brain section (108 ± 32), control brain section (76 ± 13), and an area of background (51 ± 10) of similar area (*SI Appendix*, Fig. S2).

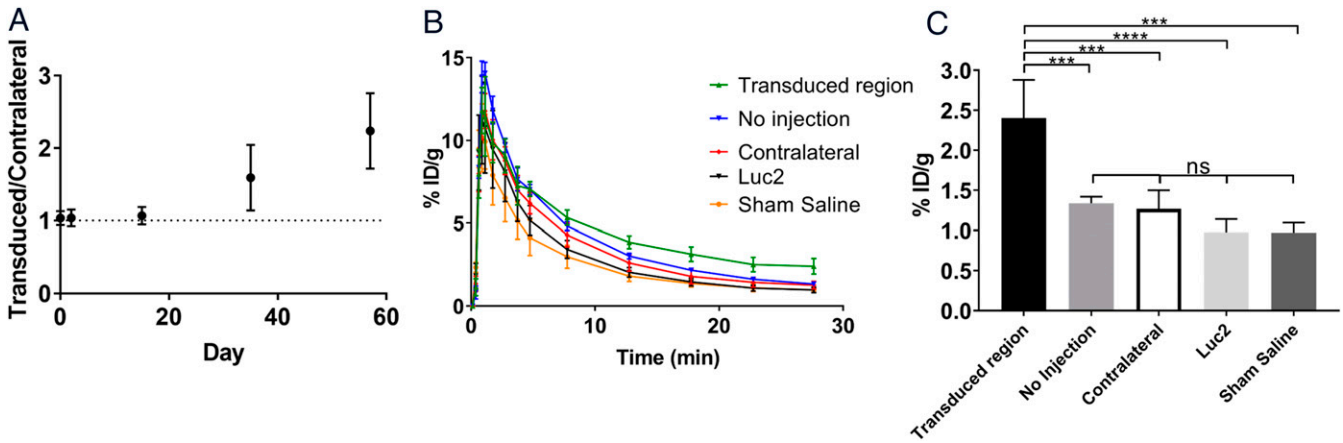

Fig. 3. (*A*) Ratio of PET signal in the transduced region to the contralateral region as a function of time after stereotactic injection of AAV-PKM2 ($n = 3$–4). Dotted line represents 1:1 ratio of normal brain to transduced region. (*B*) Time activity curves over 30 min of dynamic PET scans 57 d after administration of the AAV or controls. (*C*) Comparison of uptake values at 30 min between AAV-PKM2 transduced region ($n = 4$), contralateral control ($n = 4$), no injection ($n = 4$), AAV-Luc2 transduced region ($n = 4$), and sham injection ($n = 2$). Error bars represent SD [AAV-PKM2 transduced region vs. no injection ($P = 0.0007$, ***), AAV-PKM2 transduced region vs. contralateral ($P = 0.0004$, ***), AAV-PKM2 transduced region vs. AAV-Luc2 ($P < 0.0001$, ****), AAV transduced region vs. sham saline ($P = 0.0003$, ***), no injection vs. contralateral control ($P = 0.9962$, ns), no injection vs. AAV-Luc2 transduced region ($P = 0.3738$, ns), no injection vs. sham saline ($P = 0.5498$, ns), contralateral control vs. Luc2 ($P = 0.564$, ns), contralateral control vs. sham saline ($P = 0.7165$, ns), Luc2 vs. sham saline ($P > 0.9999$, ns)].

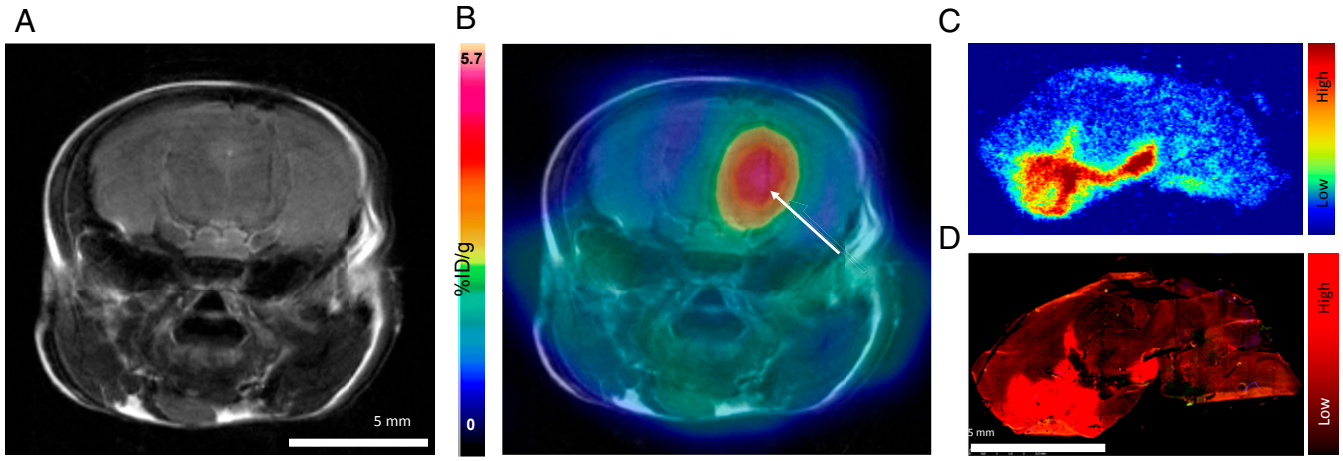

Fig. 4. (*A*) Representative T2-weighted MR coronal image of AAV transduced mouse brain. (*B*) Corresponding merged [^{18}F]DASA-23 PET/MR images (5–30 min summed [^{18}F]DASA-23 activity). White arrow indicates regions of radiotracer uptake, corresponding to the transduced region. (*C*) Ex vivo autoradiography of sagittal mouse brain sections excised 1 h after radiotracer administration. (*D*) An immunofluorescence staining for PKM2 protein in adjacent sagittal mouse brain section in *C*.

Adjacent immunofluorescence sections showed increased areas of PKM2 protein expression in AAV transduced mice (Fig. 4*D*), consistent with areas of increased radioactive signal in autoradiography sections. Control sections showed no areas of increased tracer accumulation, as did sections taken from regions that were not transduced by the AAV. Analysis of the images using ImageJ showed a statistical significance ($P > 0.0001$) between corrected total cell fluorescence (CTCF) of lowest and highest areas of signal in the brain sections transduced. However, no statistical significance was seen between any of the regions from the control sample (*SI Appendix*, Fig. S3).

Using another cohort of mice ($n = 8$) stereotactically injected with AAV9-PKM2 identically to the previous cohort, [^{18}F]DASA-23 imaging was carried out 57 d after AAV injection. Immediately after PET imaging, brains were excised and analyzed for PKM2 mRNA. A positive correlation between PKM2 mRNA levels and [^{18}F]DASA-23 PET signal was seen (Fig. 5; $R^2 = 0.66$, $P = 0.026$).

Discussion

This study evaluated the utility of PKM2 as a potential PET reporter gene in the murine brain, using [^{18}F]DASA-23 as the PET reporter probe (radiotracer). The experiments show that PKM2 protein can be successfully overexpressed, relative to controls, via AAV9-PKM2 gene delivery and that gene expression can be serially monitored using [^{18}F]DASA-23 PET imaging.

Initial cell culture studies were carried out with plasmids to simulate AAV delivery and transient gene expression and to confirm that [^{18}F]DASA-23 accumulation was due to the expression of the PKM2 reporter gene. HeLa cells were chosen for these studies as they have been shown to respond well to transfection and transduction (17), although a cancer cell line and one that already expresses PKM2, the ability to further up-regulate the protein in the cells, was seen as a promising sign for up-regulating in cell types with low endogenous gene expression. The key focus was to demonstrate that the overexpression and detection of PKM2 protein was possible in cell culture and that varying the concentration of plasmid resulted in varying PKM2 levels. The studies carried out showed that overexpression of PKM2 was straightforward and the concentration of plasmid correlated well with expression of PKM2, as confirmed by uptake studies of [^{18}F]DASA-23 and mRNA expression quantitation by real-time qPCR.

Delivery of a gene can be achieved in a number of ways, either viral or nonviral. Nonviral vectors (e.g., liposomes, exosomes, and polymeric nanoparticles) are attractive due to their simple production, low cost, and safety profile (18, 19). However, they produce relatively low expression and require repeated administration (20). Viral approaches for transduction in the CNS predominantly consist of either AAV or lentiviral delivery (21). Both have a limited genome capacity compared with adenovirus and herpes simplex virus. However, they have significant advantages in terms of long-lasting expression, no known toxicity, and low immunogenicity. Between AAVs and lentiviruses, AAVs inherently have a better safety profile due to their nonpathogenic nature of the wild-type form (20), although recent trials have used lentivirus to deliver genetic therapy in children (22). Importantly however AAVs usually induce higher transgene expression levels than lentivirus (23).

There are 12 natural serotypes of AAV and many more variants which have been isolated (24). Of the natural serotype, AAV9 has been shown to have the highest distribution through

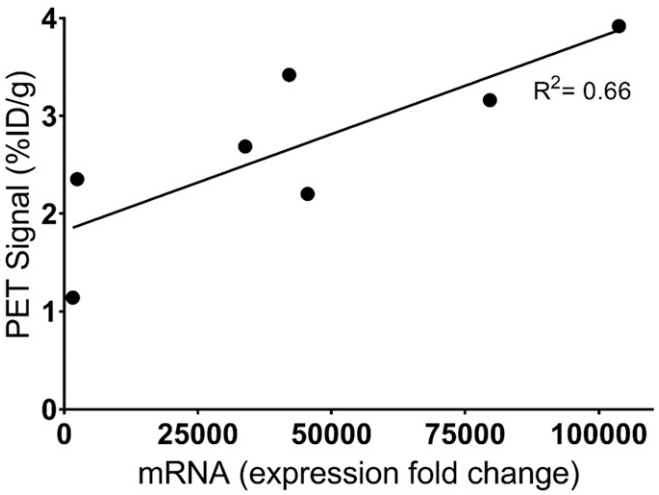

Fig. 5. PKM2 mRNA expression in the brains of transduced mice ($n = 7$) were measured by qPCR and normalized to β-actin. Relative normalized expression of individual mice plotted against [^{18}F]DASA-23 PET signal in the transduced region of the brain, at 30 min postinjection ($R^2 = 0.66$, $P = 0.026$).

the CNS, following either direct stereotactic injection or IV injection (25). AAV9 is one of the few serotype suitable for IV injection as it is capable of freely crossing the BBB (26). Although the mechanism for this is unknown, it is understood that the process is likely that of active transport rather than passive diffusion (27, 28). AAV9 has been shown to give widespread transduction of neurons and glial cells, as well as transduction of astrocytes.

Promoter choice is also an important factor when designing a reporter gene system; for this study, EF1a (*SI Appendix*, Fig. S4) was chosen due to its relatively small size (1,179 bp), an important factor considering the small cargo size available in AAVs and also as it is not readily silenced as with similar promoters such as CMV, and finally due to its ubiquitous nature as a promoter (29–31).

As both the ability of AAV9 and DASA-23 to freely cross the BBB have been previously reported (14, 25), in this study the AAV was administered to mice via stereotactic brain injection rather than IV. This is due to the high numbers of viral genome copy needed for IV administration and also to give a clearly defined region of PKM2 protein expression within the brain by PET imaging. The number of viral genome copies administered in this study were in line with previously reported studies using AAVs in the mouse brain. Further studies in progress will examine the distribution and expression of the PKM2 protein in the CNS when the AAV is administered via IV injection.

Unlike many viral delivery systems, AAVs typically take between 2 and 4 wk to show noticeable expression in vivo (32). This is due to AAVs being nonintegrating and requiring time to replicate in the cytosol before sufficient expression levels are observable (33). Although not the focus of this study, this time delay between transduction and expression was clearly seen over the serial PET imaging period utilized. Following mice throughout the duration of the study, a gradual and steady increase in the ratio of radiotracer uptake in the transduced region compared with the contralateral brain was seen over the imaging period. This is consistent with expression times previously reported (32, 34) and highlights the clear and detectable signal over time (Fig. 3*A*). No significant accumulation of [^{18}F]DASA-23 was observed in any of the control groups (Luc2 AAV, sham saline injection, no injection). This indicates that increased expression of the PKM2 protein is due to transduction by the AAV9-PKM2 virus and not another source. BLI of mice transduced with AAV-Luc2 showed bioluminescent signal, indicating that the transduction had been successful, while no bioluminescent signal was observed as expected in a mouse transduced with AAV-PKM2, which in this case is acting as a negative control due to the lack of fluorescent or bioluminescent reporter gene.

For mice that showed no significant increase in PET signal post AAV-PKM2 transduction, this may be attributed to two possible reasons. Firstly, the diffusive nature of AAV9 may successfully transduce the brain, but in such a dispersed manner that a PET signal is not visible. Secondly, it is possible that the AAV delivery in these mice did not successfully transduce the cells. The reason for this is not clear but highlights the importance of reporter gene imaging in an AAV gene therapy as there can be significant biological variation. In cases where the AAV infection is not successful, a reporter gene system would be capable of detecting this relatively early in the treatment time course. This is of particular importance in humans where anti-AAV neutralizing antibodies are found in 47% of individuals, potentially restricting the therapeutic effect of AAV vectors (35).

PKM2 protein has been widely reported on for its up-regulation in tumors and its role in their metabolic process and the rapid division of cells (9, 10, 36). It has also been shown to be up-regulated in not just cancer, but also other diseases where rapid cell proliferation is a factor (37, 38). For the majority of CNS diseases that could be potential targets for gene therapies, multiple sclerosis, Parkinson's disease, ALS, and others, increased cell proliferation and metabolism are not defining symptoms (39); therefore, PKM2 protein levels in the brain are expected to be low as in the healthy brain. This suggests that the diseased cells being treated should not give a confounding [^{18}F]DASA-23 PET signal due to PKM2 protein, which may be misinterpreted for that of reporter gene expression. However, more recently there is evidence to suggest that PKM2 protein also plays a role in the inflammatory response (40). Although PKM2 is up-regulated in many cancers it is not itself oncogenic (41), it is up-regulated in many healthy tissues outside of the CNS with important roles in cell proliferation. It remains, however, an important potential downfall and must be studied in more detail.

The other PET reporter gene systems that have been used to monitor gene expression and gene therapy are not suitable for use in the CNS. These include herpes simplex virus type 1 thymidine kinase (HSV1-tk) (42) and its mutant (HSV1-sr38tk) (43), dopamine-2 receptor (D2R) (44) and its mutant (D2R80A) (45), type 2 cannabinoid receptor mutant (4), sodium iodide symporter (NIS) (46), and the somatostatin receptor 2 (47). Of these, only D2R80A and HSV1-tk have been used within the CNS, and only the latter in a clinical setting (48). A key limitation of HSV1-tk is that its corresponding radiotracers are currently not capable of crossing the BBB due to their physiochemical properties, namely low lipophilicity. Previous studies involving HSV1-tk in the brain have been in the setting of glioblastoma where the integrity of the BBB is known to be compromised (48). D2R80A, or type 2 cannabinoid receptor, is perhaps better suited for use in the CNS as its radiotracers are capable of crossing the BBB (4, 34). However, high levels of endogenous D2R are found in the striatum (49), greatly limiting the use of this PET reporter gene system in nearby regions, while cannabinoid receptor type 2 has well documented up-regulation in activated microglia (4), limiting its use in diseases which involve neuroinflammation.

An increase in PET signal was only observed in mice that were injected with AAV-PKM2, with none being observed in any of the control groups. A lack of any increased [^{18}F]DASA-23 uptake in the brain in any of the control or AAV-PKM2 mice at 2 d suggests inflammation does not up-regulate PKM2. If this were the case, an increase in [^{18}F]DASA-23 signal would be expected to be seen around the injection site due to the significant inflammation in the localized area caused by the stereotactic injection and surgical procedure. However, a full neuroinflammation model and analysis should be carried out in the future.

To our knowledge, there has only been one PET tracer reported for the imaging of PKM2 expression, specifically DASA-23 that was developed and validated by our laboratories at Stanford. This tracer has been radiolabeled with both [^{11}C] and [^{18}F] (12–14). As the molecule is structurally identical for both isotopic forms, the ^{18}F version was chosen since the longer half-life of ^{18}F (109 min vs. 20 min for ^{11}C) facilitates the workflow for imaging living subjects. [^{18}F]DASA-23 is currently undergoing phase I clinical trials by our laboratories at Stanford to evaluate PKM2 expression in patients with intracranial tumors or recurrent glioblastoma (15). Although previously demonstrated (13, 14), the specificity of DASA-23 binding to PKM2 protein in the CNS was confirmed by immunofluorescence staining and the excellent correlation with the radioactive signal from adjacent autoradiography sections. Further confirmation was also seen in correlation between PKM2 mRNA expression and [^{18}F]DASA-23 PET signal in a separate cohort of mice transduced with PKM2-AAV9. One mRNA data point was excluded from the analysis. This mouse showed a clear PET signal but very low corresponding PKM2 mRNA expression, in line with control samples. It is likely that this disparity is due to the tissue selection for mRNA analysis missing the transduced region.

Although not studied in the current work, one would utilize the PKM2 reporter gene to monitor expression of another gene

being delivered into the brain (50). This approach would utilize a vector in which expression of the therapeutic gene of interest is coupled to the PKM2 PET reporter gene, allowing indirect assessment of therapeutic gene expression with [^{18}F]DASA-23 PET imaging.

Conclusions

Herein we have investigated the utility of PKM2 and its corresponding radiotracer [^{18}F]DASA-23 as a potential PET reporter gene/reporter probe system for use in the CNS. Cell culture studies showed that PKM2 protein levels could be successfully increased in HeLa cells by transfection with a PKM2-containing plasmid. PKM2 expression levels, as measured by radiotracer uptake studies and mRNA levels, correlated well with the amount of plasmid used for transfection during the transfection procedure.

In vivo studies showed an increase in PKM2 protein expression in the brain over 2 mo, following stereotactic injection of an AAV9 containing the PKM2 gene. The increase in expression was confirmed by dynamic PET imaging, mRNA analysis, autoradiography, and immunofluorescence, and revealed that PKM2 has the potential to be further developed into a PET/[^{18}F]DASA-23 reporter gene/reporter probe system for the imaging of gene therapy.

ACKNOWLEDGMENTS. We thank the Radiochemistry facility at Stanford University for the ^{18}F production and the Stanford Gene Vector and Virus Core for the purification and packaging of the AAV viruses. We acknowledge the Stanford Center for Innovation in In-Vivo Imaging for supporting the preclinical imaging experiments and image analyses. This work was funded in part by a grant from Biogen Inc., Cambridge, MA (to S.S.G.) and also in part by the Ben and Catherine Ivy Foundation (to S.S.G.).

1. K. Shah, A. Jacobs, X. O. Breakefield, R. Weissleder, Molecular imaging of gene therapy for cancer. *Gene Ther.* **11**, 1175–1187 (2004).
2. First in vivo human genome editing trial. *Nat. Biotechnol.* **36**, 5 (2018).
3. I. Peñuelas, U. Haberkorn, S. Yaghoubi, S. S. Gambhir, Gene therapy imaging in patients for oncological applications. *Eur. J. Nucl. Med. Mol. Imaging* **32** (Suppl 2), S384–S403 (2005).
4. C. Vandeputte *et al.*, A PET brain reporter gene system based on type 2 cannabinoid receptors. *J. Nucl. Med.* **52**, 1102–1109 (2011).
5. S. S. Yaghoubi, D. O. Campbell, C. G. Radu, J. Czernin, Positron emission tomography reporter genes and reporter probes: Gene and cell therapy applications. *Theranostics* **2**, 374–391 (2012).
6. P. W. Miller, N. J. Long, R. Vilar, A. D. Gee, Synthesis of 11C, 18F, 15O, and 13N radiolabels for positron emission tomography. *Angew. Chem. Int. Ed. Engl.* **47**, 8998–9033 (2008).
7. A. H. Jacobs, C. Dittmar, A. Winkeler, G. Garlip, W. D. Heiss, Molecular imaging of gliomas. *Mol. Imaging* **1**, 309–335 (2002).
8. R. Weissleder, A. Rehemtulla, S. S. Gambhir, *Molecular Imaging: Principles and Practice* (People's Medical Publishing House, 2010).
9. N. Wong, J. De Melo, D. Tang, PKM2, a central point of regulation in cancer metabolism. *Int. J. Cell Biol.* **2013**, 242513 (2013).
10. J. Mukherjee *et al.*, Pyruvate kinase M2 expression, but not pyruvate kinase activity, is up-regulated in a grade-specific manner in human glioma. *PLoS One* **8**, e57610 (2013).
11. W. Luo, G. L. Semenza, Emerging roles of PKM2 in cell metabolism and cancer progression. *Trends Endocrinol. Metab.* **23**, 560–566 (2012).
12. C. Beinat *et al.*, The utility of [^{18}F]DASA-23 for molecular imaging of prostate cancer with positron emission tomography. *Mol. Imaging Biol.* **20**, 1015–1024 (2018).
13. C. Beinat, I. S. Alam, M. L. James, A. Srinivasan, S. S. Gambhir, Development of [^{18}F]DASA-23 for imaging tumor glycolysis through noninvasive measurement of pyruvate kinase M2. *Mol. Imaging Biol.* **19**, 665–672 (2017).
14. T. H. Witney *et al.*, PET imaging of tumor glycolysis downstream of hexokinase through noninvasive measurement of pyruvate kinase M2. *Sci. Transl. Med.* **7**, 310ra169 (2015).
15. C. Beinat *et al.*, [18F]DASA-23 and PET scan in evaluating pyruvate kinase M2 expression in patients with intracranial tumors or recurrent glioblastoma and healthy volunteers. Full Text View–ClinicalTrials.gov. https://www.clinicaltrials.gov/ct2/show/NCT03539731?term=DASA&cond=Glioblastoma&cntry=US&state=US%3ACA&rank=1. Accessed 29 June 2018.
16. D. Anastasiou *et al.*, Pyruvate kinase M2 activators promote tetramer formation and suppress tumorigenesis. *Nat. Chem. Biol.* **8**, 839–847 (2012).
17. E. J. Dunphy, R. A. Redman, H. Herweijer, T. P. Cripe, Reciprocal enhancement of gene transfer by combinatorial adenovirus transduction and plasmid DNA transfection in vitro and in vivo. *Hum. Gene Ther.* **10**, 2407–2417 (1999).
18. M. Conceição *et al.*, Intravenous administration of brain-targeted stable nucleic acid lipid particles alleviates Machado-Joseph disease neurological phenotype. *Biomaterials* **82**, 124–137 (2016).
19. L. Alvarez-Erviti *et al.*, Delivery of siRNA to the mouse brain by systemic injection of targeted exosomes. *Nat. Biotechnol.* **29**, 341–345 (2011).
20. J. Saraiva, R. J. Nobre, L. Pereira de Almeida, Gene therapy for the CNS using AAVs: The impact of systemic delivery by AAV9. *J. Control. Release* **241**, 94–109 (2016).
21. R. J. Nobre, L. P. Almeida, Gene therapy for Parkinson's and Alzheimer's diseases: From the bench to clinical trials. *Curr. Pharm. Des.* **17**, 3434–3445 (2011).
22. F. Eichler *et al.*, Hematopoietic stem-cell gene therapy for cerebral adrenoleukodystrophy. *N. Engl. J. Med.* **377**, 1630–1638 (2017).
23. A. P. Kells *et al.*, Efficient gene therapy-based method for the delivery of therapeutics to primate cortex. *Proc. Natl. Acad. Sci. U.S.A.* **106**, 2407–2411 (2009).
24. G. Gao *et al.*, Clades of Adeno-associated viruses are widely disseminated in human tissues. *J. Virol.* **78**, 6381–6388 (2004).
25. C. N. Cearley, J. H. Wolfe, A single injection of an adeno-associated virus vector into nuclei with divergent connections results in widespread vector distribution in the brain and global correction of a neurogenetic disease. *J. Neurosci.* **27**, 9928–9940 (2007).
26. K. D. Foust *et al.*, Rescue of the spinal muscular atrophy phenotype in a mouse model by early postnatal delivery of SMN. *Nat. Biotechnol.* **28**, 271–274 (2010).
27. S. J. Gray *et al.*, Preclinical differences of intravascular AAV9 delivery to neurons and glia: A comparative study of adult mice and nonhuman primates. *Mol. Ther.* **19**, 1058–1069 (2011).
28. F. P. Manfredsson, A. C. Rising, R. J. Mandel, AAV9: A potential blood-brain barrier buster. *Mol. Ther.* **17**, 403–405 (2009).
29. A. R. Brooks *et al.*, Transcriptional silencing is associated with extensive methylation of the CMV promoter following adenoviral gene delivery to muscle. *J. Gene Med.* **6**, 395–404 (2004).
30. I. Sinici, M. Zarghooni, M. B. Tropak, D. J. Mahuran, H. A. Özkara, Comparison of HCMV IE and EF-1 promoters for the stable expression of β-subunit of hexosaminidase in CHO cell lines. *Biochem. Genet.* **44**, 173–180 (2006).
31. J. Y. Qin *et al.*, Systematic comparison of constitutive promoters and the doxycycline-inducible promoter. *PLoS One* **5**, e10611 (2010).
32. Q. Chen *et al.*, Recombinant adeno-associated virus serotype 9 in a mouse model of atherosclerosis: Determination of the optimal expression time in vivo. *Mol. Med. Rep.* **15**, 2090–2096 (2017).
33. S. Daya, K. I. Berns, Gene therapy using adeno-associated virus vectors. *Clin. Microbiol. Rev.* **21**, 583–593 (2008).
34. S. Y. Yoon *et al.*, Quantitative, noninvasive, in vivo longitudinal monitoring of gene expression in the brain by co-AAV transduction with a PET reporter gene. *Mol. Ther. Methods Clin. Dev.* **1**, 14016 (2014).
35. N. Miyake, K. Miyake, M. Yamamoto, Y. Hirai, T. Shimada, Global gene transfer into the CNS across the BBB after neonatal systemic delivery of single-stranded AAV vectors. *Brain Res.* **1389**, 19–26 (2011).
36. W. J. Israelsen *et al.*, PKM2 isoform-specific deletion reveals a differential requirement for pyruvate kinase in tumor cells. *Cell* **155**, 397–409 (2013).
37. T. Shirai *et al.*, The glycolytic enzyme PKM2 bridges metabolic and inflammatory dysfunction in coronary artery disease. *J. Exp. Med.* **213**, 337–354 (2016).
38. M. L. Rees *et al.*, A PKM2 signature in the failing heart. *Biochem. Biophys. Res. Commun.* **459**, 430–436 (2015).
39. B. Spencer *et al.*, Systemic central nervous system (CNS)-targeted delivery of neuropeptide Y (NPY) reduces neurodegeneration and increases neural precursor cell proliferation in a mouse model of Alzheimer disease. *J. Biol. Chem.* **291**, 1905–1920 (2016).
40. J. C. Alves-Filho, E. M. Pålsson-McDermott, Pyruvate kinase M2: A potential target for regulating inflammation. *Front. Immunol.* **7**, 145 (2016).
41. M. A. Iqbal, V. Gupta, P. Gopinath, S. Mazurek, R. N. K. Bamezai, Pyruvate kinase M2 and cancer: An updated assessment. *FEBS Lett.* **588**, 2685–2692 (2014).
42. S. S. Gambhir *et al.*, Imaging adenoviral-directed reporter gene expression in living animals with positron emission tomography. *Proc. Natl. Acad. Sci. U.S.A.* **96**, 2333–2338 (1999).
43. S. S. Gambhir *et al.*, A mutant herpes simplex virus type 1 thymidine kinase reporter gene shows improved sensitivity for imaging reporter gene expression with positron emission tomography. *Proc. Natl. Acad. Sci. U.S.A.* **97**, 2785–2790 (1999).
44. D. C. MacLaren *et al.*, Repetitive, non-invasive imaging of the dopamine D2 receptor as a reporter gene in living animals. *Gene Ther.* **6**, 785–791 (1999).
45. Q. Liang *et al.*, Noninvasive, quantitative imaging in living animals of a mutant dopamine D2 receptor reporter gene in which ligand binding is uncoupled from signal transduction. *Gene Ther.* **8**, 1490–1498 (2001).
46. A. Khoshnevisan *et al.*, 18F-Fluorosulfate for PET imaging of the sodium-iodide symporter: Synthesis and biologic evaluation in vitro and in vivo. *J. Nucl. Med.* **58**, 156–161 (2017).
47. A. Becherer *et al.*, Imaging of advanced neuroendocrine tumors with (18)F-FDOPA PET. *J. Nucl. Med.* **45**, 1161–1167 (2004).
48. K. V. Keu *et al.*, Reporter gene imaging of targeted T cell immunotherapy in recurrent glioma. *Sci. Transl. Med.* **9**, eaag2196 (2017).
49. X. Wei *et al.*, Dopamine D1 or D2 receptor-expressing neurons in the central nervous system. *Addict. Biol.*, **23** 569–584 (2018).
50. Y. Yu *et al.*, Quantification of target gene expression by imaging reporter gene expression in living animals. *Nat. Med.* **6**, 933–937 (2000).